Neutron Diffraction Study of the Cation Distributions in the Systems $Fe_{7-x}M_x(PO_4)_6$ (M = Mn or Co)

Philip Lightfoot and Anthony K. Cheetham *
University of Oxford, Chemical Crystallography Laboratory, 9 Parks Road, Oxford OX1 3PD

The cation distributions in the mixed-metal phosphate systems $Fe_{7-x}M_x(PO_4)_6$ [(**1**) M = Mn, $x = 2$; (**2**) M = Co, $x = 3$] have been studied by Rietveld analysis of powder neutron diffraction data. Both systems are synthesised hydrothermally, with subsequent low-temperature (500 °C) annealing. They adopt the $Fe_7(PO_4)_6$ structure type, which provides four crystallographically distinct metal sites, three of which are octahedral and one five-co-ordinated. Iron is found to be preferentially oxidised over the dopant cation in both cases, giving idealised compositions '$Fe^{II}Fe^{III}_4Mn^{II}_2(PO_4)_6$' and '$Fe^{III}_4Co^{II}_3(PO_4)_6$.' The cation sites are found to be strongly ordered, with Fe^{3+} preferentially occupying the two most distorted octahedral sites, rather than the more regular octahedral site and the five-co-ordinated (trigonal bipyramidal) site, in both cases. These observations may be rationalised in terms of a balance of coulombic, ligand-field, and other considerations.

Phosphates of the first-row transition metals adopt a wide variety of stoicheiometries and structure types, and have a similarly large number of properties and applications. For example, $KTiO(PO_4)$[1] is well known for its non-linear optical properties, whilst phases based on the Nasicon framework, such as $Na_3Cr_2(PO_4)_3$,[2] exhibit fast ionic conduction, and several of the vanadium phosphates are active in oxidation catalysis.[3] Despite this, however, many of these phase diagrams have been relatively poorly explored, and the consequent scope for preparing new and potentially interesting materials is very wide. We have recently demonstrated this by the synthesis of two new layer-type phosphates involving Mn^{3+}, $KMn_2O(PO_4)(HPO_4)$[4] and $NH_4Mn_2O(PO_4)(HPO_4)\cdot H_2O$.[5] Amongst other new phases we have synthesised are the hydrogenphosphates $Mn_7(PO_4)_2(HPO_4)_4$ and $Co_7(PO_4)_2(HPO_4)_4$,[6,7] both of which contain the transition metal in the purely bivalent state, and a partially oxidised analogue, $Fe_7(PO_4)_3(HPO_4)_3$, containing both Fe^{2+} and Fe^{3+}.[6] All these phases are related to the mixed-valence iron phosphate $Fe^{II}_3Fe^{III}_4(PO_4)_6$,[8] the hydrogenous phases differing in having H atoms added to the basic $M_7(PO_4)_6$ framework in the form of M–(OH)–P groups. The $Fe_7(PO_4)_6$ structure itself is quite complex (Figure 1), having four crystallographically distinct metal sites, three of which are six- and one five-co-ordinated. These sites are sufficiently different in character that complete ordering of Fe^{2+}/Fe^{3+} takes place, with Fe^{2+} occupying the more regular octahedral M(1) site and the distorted trigonal bipyramidal M(3) site in preference to the more distorted octahedral M(2) and M(4) sites. The possibility of synthesising mixed phases $Fe_{7-x}M_x(PO_4)_{6-y}(HPO_4)_y$ ($y = 0$—4) clearly introduces further complexity into the system, and a detailed investigation of the whole system as a function of the variables M, x, and y would be a considerable undertaking. By limiting these variables to the case where $y = 0$ and M = Mn or Co, we may hope to study the oxidation states of the cations present in the system, Fe and M, and their ordering over the available sites. In this study we therefore set out to prepare fully oxidised samples, $Fe_{7-x}M_x(PO_4)_6$, and to determine the occupancies of the cation sites. This is best studied by neutron diffraction, due to the relative scattering powers of the elements concerned [b(Fe) = 0.95×10^{-14}, b(Mn) = -0.39×10^{-14}, and b(Co) = 0.25×10^{-14}m),[9] which clearly leads to a better discrimination of the elements than would be achieved with X-rays.

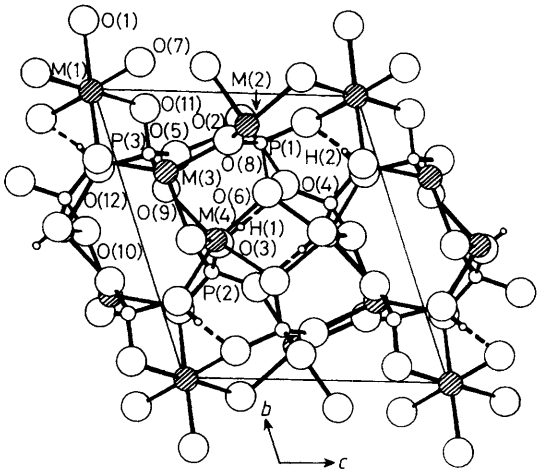

Figure 1. A projection of the structure of $Fe_{7-x}M_x(PO_4)_6$ down a^*

Experimental

Synthesis and Characterisation.—Phases in the solid solutions $Fe_{7-x}Mn_x(PO_4)_6$ and $Fe_{7-x}Co_x(PO_4)_6$ may be prepared by a two-step process. The first stage involves hydrothermal synthesis of $Fe_{7-x}M_x(PO_4)_{6-y}(HPO_4)_y$ ($y = 0$—4). The precise compositions of these phases are not well determined, and depend on the exact experimental conditions employed. However, on heating in air to 400—500 °C they are oxidised to idealised stoicheiometries $Fe_{7-x}M_x(PO_4)_6$. The actual conditions of synthesis were as follows.

(**1**; M = Mn, x = 2). A stoicheiometric mixture of $MnSO_4\cdot H_2O$, $FeSO_4\cdot 7H_2O$, and $NH_4H_2PO_4$, sufficient to make up 10 g total, was added to distilled water (15 cm^3) and sealed in a Teflon-lined stainless-steel autoclave. The mixture was heated at 220 °C for 48 h, and subsequently cooled to room temperature. The product, a dark green polycrystalline material, was isolated by suction filtration and dried in air at room temperature. X-Ray powder diffraction (X-r.p.d.) revealed the product to be a homogeneous $Fe_7(PO_4)_6$-like phase. The sample was then heated at 450 °C for 1 h, whereupon the product was again analysed by X-r.p.d. Very little shift in the

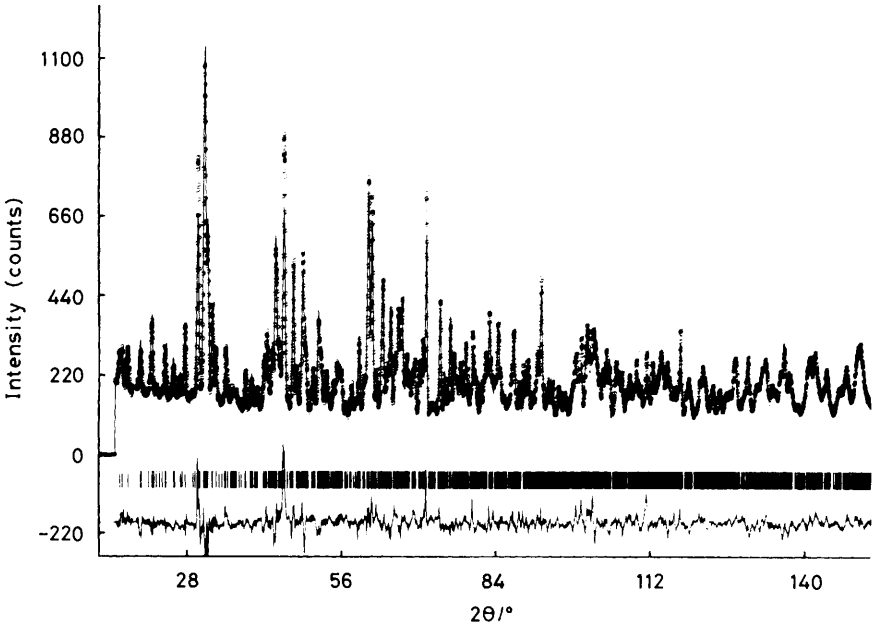

Figure 2. The observed (open circles), calculated (smooth curve), and difference (below) neutron diffraction profiles for $(Fe,Mn)_7(PO_4)_6$; reflection positions are marked

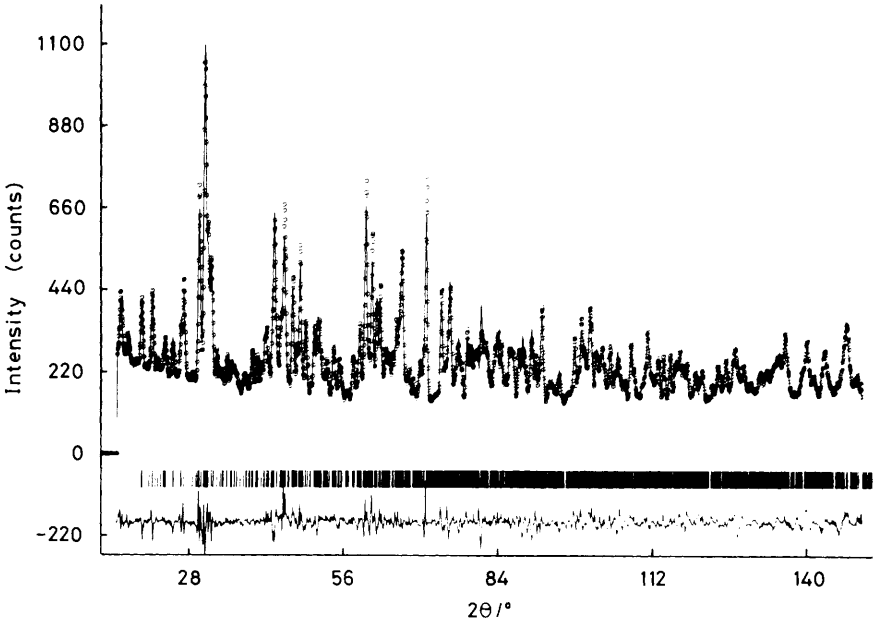

Figure 3. The observed (open circles), calculated (smooth curve), and difference (below) neutron diffraction profiles for $(Fe,Co)_7(PO_4)_6$; reflection positions are marked

reflection positions could be observed, which suggested, together with the fact that there was no observable colour change in the product, that the phase from the hydrothermal synthesis was almost completely oxidised originally.

(**2**; M = Co, x = 3). This sample was prepared by a method analogous to that described above. The starting point was a stoicheiometric mixture of $FeSO_4 \cdot 7H_2O$, $CoCl_2 \cdot 6H_2O$, and $NH_4H_2PO_4$. In this case, the product of the hydrothermal synthesis was a purple polycrystalline solid, which was oxidised to a dull green phase on annealing at 450 °C for 1 h. It was apparent, both from the colour change and from the *X*-r.p.d., that a significant degree of oxidation had occurred during the annealing process.

Data Collection and Refinement.—Room-temperature neutron diffraction data were collected on the high-resolution powder diffractometer D2b at the Laue–Langevin Institute (ILL), Grenoble. Approximately 8 g of sample were placed in an 8-mm vanadium can, and data were collected in the range $6 < 2\theta < 156°$, at intervals of 0.05° in the case of compound (**1**) and 0.025° in the case of compound (**2**). A mean neutron wavelength of 1.594 6(5) Å was used for both experiments.

Data analysis by the Rietveld technique[10] used a program modified by Cox[11] to incorporate the pseudo-Voigt[12] peak shape. Atomic co-ordinates from the single-crystal refinement of $Co_7(PO_4)_2(HPO_4)_4$[7] were used as a starting model for both refinements. Due to the complexity of the problem, the refinements proceeded rather slowly, parameters being added gradually and with heavily damped shifts. During the final cycles, a total of 72 least-squares parameters were refined for (**1**), 74 for (**2**), with more than 1 600 contributing reflections in both cases.

Table 1. Final profile parameters for the Rietveld refinements of $(Fe,Mn)_7(PO_4)_6$ (**1**) and $(Fe,Co)_7(PO_4)_6$ (**2**)

	(1)	(2)
Unit cell constants (space group $P\bar{1}$)		
	a/Å 6.365(1)	6.350(1)
	b/Å 9.327(2)	9.300(2)
	c/Å 8.069(2)	7.915(2)
	α/° 105.25(1)	104.70(1)
	β/° 101.90(1)	101.52(1)
	γ/° 108.16(1)	108.47(1)
Profile parameters (0.001°)[11]		
	U 125 000(7000)	85 000(5 000)
	V −185 000(15 000)	−132 000(9 000)
	W 263 000(6000)	168 000(4 000)
		X −9(7)
		Y 45(2)
	Zero point 183(3)	307(2)
	Asymmetry parameter 0.80 × 10^{-6}	2.43(8) × 10^{-6}
R factors[10]		
	R_{nuc} 0.0611	0.0912
	R_{pr} 0.1065	0.1264
	R_{wp} 0.1235	0.1509
	R_{exp} 0.0579	0.0629

Table 2. Final atomic co-ordinates for $(Fe,Mn)_7(PO_4)_6$

Atom	X/a	Y/b	Z/c	Occupancy
Fe(1)	0	0	0	0.082(5)
Mn(1)	0	0	0	0.418(5)
Fe(2)	0.380 4(9)	0.111 8(6)	0.455 5(7)	1.000(9)
Mn(2)	0.380 4(9)	0.111 8(6)	0.455 5(7)	0.000(9)
Fe(3)	0.256(5)	0.293(4)	−0.229(4)	0.396(7)
Mn(3)	0.256(5)	0.293(4)	−0.229(4)	0.604(7)
Fe(4)	0.046 8(9)	−0.468 2(6)	−0.275 1(6)	0.992(9)
Mn(4)	0.046 8(9)	−0.468 2(6)	−0.275 1(6)	0.008(9)
P(1)	0.101(2)	−0.162(1)	−0.402(1)	
P(2)	0.396(1)	0.366(1)	0.233(1)	
P(3)	0.224(2)	−0.235 6(9)	0.154(1)	
O(1)	0.276(1)	0.240 3(9)	0.043(1)	
O(2)	0.312(1)	−0.081(1)	−0.458(1)	
O(3)	0.252(2)	0.463(1)	0.289(1)	
O(4)	0.449(1)	0.283 4(9)	0.361(1)	
O(5)	0.460(1)	−0.225(1)	0.273(1)	
O(6)	0.071(1)	−0.347(1)	−0.448(1)	
O(7)	0.127(1)	−0.077 0(9)	−0.210(1)	
O(8)	0.122(2)	0.161(1)	−0.467(1)	
O(9)	−0.019(2)	0.343(1)	−0.193(1)	
O(10)	0.371(1)	−0.489(1)	−0.241(1)	
O(11)	0.218(2)	−0.067(1)	0.198(1)	
O(12)	0.205(1)	−0.297(1)	−0.046(1)	

Isotropic thermal parameters (Å^2): Fe,Mn,P 0.61(4); O, 0.87(3).

Results and Discussion

Final observed, calculated, and difference profiles for compounds (**1**) and (**2**) are given in Figures 2 and 3, respectively, and the refined profile parameters for both compounds are given in Table 1. Final atomic co-ordinates and selected bond distances, together with associated bond strengths,[13] are given in Tables 2—5. The relatively large R factors in both refinements are in part due to the modest signal-to-noise ratio of the data and also due to the fact that the monochromator on the D2b instrument is imperfect, leading to a non-Gaussian peak shape that is difficult to fit in a simple way. This problem is partly overcome, in the case of compound (**1**), by the use of a larger (0.05 *vs.* 0.025°) step size in the scan and, in the case of compound (**2**), by

Table 3. Final atomic co-ordinates for $(Fe,Co)_7(PO_4)_6$

Atom	X/a	Y/b	Z/c	Occupancy
Fe(1)	0	0	0	0.118(8)
Co(1)	0	0	0	0.382(8)
Fe(2)	0.381 9(9)	0.113 1(6)	0.448 5(6)	0.86(1)
Co(2)	0.381 9(9)	0.113 1(6)	0.448 5(6)	0.14(1)
Fe(3)	0.274(2)	0.271(1)	−0.192(2)	0.07(1)
Co(3)	0.274(2)	0.271(1)	−0.192(2)	0.93(1)
Fe(4)	0.046 7(8)	−0.473 9(5)	−0.276 3(5)	1.01(1)
Co(4)	0.046 7(8)	−0.473 9(5)	−0.276 3(5)	−0.01(1)
P(1)	0.099(1)	−0.171 8(9)	−0.413 8(9)	
P(2)	0.394(1)	0.361 8(8)	0.221 3(9)	
P(3)	0.231(1)	−0.229 7(8)	0.147 7(10)	
O(1)	0.267(1)	0.234 4(8)	0.035 0(9)	
O(2)	0.315(1)	−0.072 9(8)	−0.460 7(9)	
O(3)	0.249(1)	0.463 1(8)	0.273 5(9)	
O(4)	0.448(1)	0.283 6(8)	0.362 7(9)	
O(5)	0.460(1)	−0.222 8(8)	0.272 9(10)	
O(6)	0.068(1)	−0.349 3(8)	−0.450 8(9)	
O(7)	0.123(1)	−0.080 8(8)	−0.206 6(9)	
O(8)	0.127(1)	0.167 1(8)	−0.461 4(9)	
O(9)	−0.033(1)	0.327 6(8)	−0.198 8(9)	
O(10)	0.377(1)	−0.492 0(8)	−0.228 1(9)	
O(11)	0.228(1)	−0.055 5(7)	0.196 4(9)	
O(12)	0.209(1)	−0.292 6(8)	−0.053 6(9)	

Isotropic thermal parameters (Å^2): Fe,Co,P 0.50(3); O, 0.77(2).

Table 4. Selected bond distances (Å) and bond strengths (valence units) for $(Fe,Mn)_7(PO_4)_6$

	d(M–O)	s(M–O)		d(P–O)	s(P–O)
M(1)–O(1)	2 × 2.26(2)	0.28[a]	P(1)–O(2)	1.54(2)	1.23
M(1)–O(7)	2 × 2.08(2)	0.44	P(1)–O(6)	1.60(2)	1.09
M(1)–O(11)	2 × 2.24(2)	0.29	P(1)–O(7)	1.49(2)	1.37
		—	P(1)–O(8)	1.59(2)	1.11
		2.02			—
		—			4.80
					—
M(2)–O(2)	2.05(2)	0.30[b]			
M(2)–O(2)	2.06(2)	0.30	P(2)–O(1)	1.52(2)	1.29
M(2)–O(4)	1.92(2)	0.43	P(2)–O(3)	1.54(2)	1.23
M(2)–O(5)	2.04(2)	0.31	P(2)–O(4)	1.48(2)	1.40
M(2)–O(8)	2.02(2)	0.33	P(2)–O(10)	1.54(2)	1.23
M(2)–O(11)	2.09(2)	0.27			—
		—			5.15
		2.94			—
		—			
			P(3)–O(5)	1.57(2)	1.16
M(3)–O(1)	1.91(4)	—[c]	P(3)–O(9)	1.53(2)	1.25
M(3)–O(5)	2.07(4)	—	P(3)–O(11)	1.53(2)	1.25
M(3)–O(8)	2.03(4)	—	P(3)–O(12)	1.52(2)	1.29
M(3)–O(9)	2.17(4)	—			—
M(3)–O(10)	2.19(4)	—			4.95
		—			—
		—			
		—			
M(4)–O(3)	1.90(2)	0.69[b]			
M(4)–O(6)	2.01(2)	0.50			
M(4)–O(6)	2.24(2)	0.28			
M(4)–O(9)	2.00(2)	0.52			
M(4)–O(10)	2.10(2)	0.40			
M(4)–O(12)	1.91(2)	0.66			
		—			
		3.05			
		—			

[a] Values for M(1) site calculated for 100% Mn^{2+} occupancy. [b] Values for M(2) and M(4) sites calculated for 100% Fe^{3+} occupancy. [c] Values for M(3) site not calculated due to mixed occupancy.

the use of a pseudo-Voigtian [12] peak shape. It is also possible, however, that the presence of a small amount of some otherwise unobservable impurity [particularly in the case of compound (**2**)] could account for some of the discrepancy. However, no such impurity was seen either in the *X*-ray powder patterns or by electron microscopy. Nevertheless, despite these problems, the data in Tables 4 and 5 demonstrate the chemical validity of the refinements. All the geometries lie within very reasonable limits, given the crystallographic complexity of the problem. This is best demonstrated by the PO_4 groups, which have tetrahedral angles lying in the range 102—114°, and P–O distances in the range 1.48—1.62 Å. Moreover, the major aim of the refinements, the determination of cation ordering, was achieved successfully. This is shown by both the occupancy values and estimated standard deviations (e.s.d.s) given in Tables 2 and 3, and also by the bond-strength calculations in Tables 4 and 5. In both cases, the M(2) and M(4) sites are seen to be almost wholly occupied by Fe, in the form of Fe^{3+}, with the M(1) and M(3) sites being occupied by M^{2+}. A summary of the refined site occupancies, for comparison with those in $Fe_7(PO_4)_6$, itself, is given in Table 6. The refined occupancy values lead to experimentally determined stoicheiometries '$Fe_{4.1}Co_{2.9}(PO_4)_6$' and '$Fe_{4.94}Mn_{2.06}(PO_4)_6$', in reasonable agreement with those expected on the basis of the syntheses. The bond-strength calculations show that iron is preferentially oxidised to the trivalent state in both cases, giving compositions close to the idealised ones, $Fe^{III}_4Co^{II}_3(PO_4)_6$ and $Fe^{II}Fe^{III}_4Mn^{II}_2(PO_4)_6$, assuming that no hydrogen is present in either phase.

Table 5. Selected bond distances (Å) and bond strengths (valence units) for $(Fe,Co)_7(PO_4)_6$

	d(M–O)	*s*(M–O)		*d*(P–O)	*s*(P–O)
M(1)–O(1)	2 × 2.211(7)	0.27[a]	P(1)–O(2)	1.55(2)	1.21
M(1)–O(7)	2 × 2.021(7)	0.42	P(1)–O(6)	1.50(2)	1.25
M(1)–O(11)	2 × 2.171(7)	0.29	P(1)–O(7)	1.62(2)	1.04
			P(1)–O(8)	1.56(2)	1.17
		1.96			
					4.67
M(2)–O(2)	2.01(1)	0.50[b]			
M(2)–O(2)	2.07(1)	0.44	P(2)–O(1)	1.50(2)	1.34
M(2)–O(4)	1.84(1)	0.80	P(2)–O(3)	1.56(2)	1.18
M(2)–O(5)	2.04(1)	0.46	P(2)–O(4)	1.51(2)	1.33
M(2)–O(8)	2.04(1)	0.46	P(2)–O(10)	1.56(2)	1.20
M(2)–O(11)	2.02(1)	0.50			
					5.05
		3.16			
			P(3)–O(5)	1.60(2)	1.10
M(3)–O(1)	1.91(2)	0.56[a]	P(3)–O(9)	1.51(2)	1.33
M(3)–O(5)	2.07(2)	0.38	P(3)–O(11)	1.59(2)	1.13
M(3)–O(8)	2.03(2)	0.42	P(3)–O(12)	1.52(2)	1.30
M(3)–O(9)	2.17(2)	0.30			
M(3)–O(10)	2.19(2)	0.28			4.86
		1.94			
M(4)–O(3)	1.93(1)	0.62[b]			
M(4)–O(6)	2.02(1)	0.50			
M(4)–O(6)	2.16(1)	0.34			
M(4)–O(9)	2.01(1)	0.50			
M(4)–O(10)	2.10(1)	0.40			
M(4)–O(12)	1.90(1)	0.68			
		3.04			

[a] Values for M(1) and M(3) site calculated for 100% Co^{2+} occupancy. [b] Values for M(2) and M(4) sites calculated for 100% Fe^{3+} occupancy.

The preferred oxidation of Fe over Mn or Co is not surprising, and would be expected by analogy with the appropriate solution electrode potentials. The observed cation distributions are perhaps less easily explained, but they may be rationalised by examining a number of effects, including ligand-field and coulombic considerations. Considering the latter, the site potentials given in Table 7 were calculated using the program MADELUNG,[14] assuming that each atom site is occupied by a point charge of the appropriate magnitude (−2 for O, +5 for P, and +2, +3, or a weighted average charge for the metal sites). Potentials were calculated for two idealised models: (*i*) uniform charge distribution (*i.e.* a charge of 2.57 on each metal site), and (*ii*) ordered charge distribution [*i.e.* charges of +2 at M(1) and M(3) and +3 at M(2) and M(4), as in $Fe_7(PO_4)_6$, itself[8]]. Both calculations clearly show that the site potential at the M(3) site is significantly less negative than at any of the octahedral sites and would therefore be expected to favour the less highly charged cations (in agreement with the intuitively expected outcome, due to five-co-ordination). This prediction agrees well with the observed distribution. No clear predictions may be made on this basis concerning the charge distributions on the octahedral sites, however. Nevertheless, the observed distributions may be partially understood in terms of ligand-field and related effects.

The cations that we must consider are Fe^{2+} (d^6), Fe^{3+} (d^5), Co^{2+} (d^7), and Mn^{2+} (d^5), all of which may be assumed to be high spin. Of these, Fe^{3+} and Mn^{2+} have no site preference on ligand-field grounds, whereas Co^{2+} and Fe^{2+} would be expected to show an octahedral site preference. The ligand-field stabilisation energy might be greater when these ions occupy the more distorted octahedral sites, M(2) and M(4), but this could lead to a loss of spin–orbit coupling stabilisation, and it is normally the case that such ions, with their triply degenerate ground states, will prefer regular octahedral co-ordination in the absence of magnetic ordering.[15] This is observed in the iron(II) and cobalt(II) oxides, and is consistent with a substantial concentration of Co^{2+} on site M(1) in the cobalt compound.

Table 6. Summary of metal site occupancies in $M_7(PO_4)_6$ type phases

	M(1)	M(2)	M(3)	M(4)
$Fe_7(PO_4)_6$	100% Fe^{2+} 0% Fe^{3+}	0% Fe^{2+} 100% Fe^{3+}	100% Fe^{2+} 0% Fe^{3+}	0% Fe^{2+} 100% Fe^{3+}
'$Fe^{III}_4Co^{II}_3(PO_4)_6$'	76% Co^{2+} 24% Fe^{3+}	14% Co^{2+} 86% Fe^{3+}	93% Co^{2+} 7% Fe^{3+}	0% Co^{2+} 100% Fe^{3+}
'$Fe^{II}Fe^{III}_4Mn^{II}_2(PO_4)_6$'	84% Mn^{2+} 16% Fe^{3+}	0% Mn^{2+} 100% Fe^{3+}	60% Mn^{2+} 40% Fe^{2+}	0% Mn^{2+} 100% Fe^{3+}

Table 7. Calculated metal site potentials in $M_7(PO_4)_6$ type phases

Model *	M(1)	M(2)	M(3)	M(4)
(*i*)	−2.28	−2.19	−1.88	−2.39
(*ii*)	−2.04	−2.26	−1.58	−2.43

* See text.

The factors controlling the distribution of the high-spin ions, Mn^{2+} and Fe^{3+}, over the three octahedral sites in the manganese phase remain unclear, although the results shown in Table 7 do not preclude a coulombic driving force.

Acknowledgements

We thank the S.E.R.C. for the provision of neutron diffraction facilities at ILL, Grenoble and a Studentship (for P. L.).

References

1 I. Tordjman, R. Masse, and J. C. Guitel, *Z. Kristallogr., Kristallgeom., Kristallphys., Krystallchem.*, 1974, **139**, 103.
2 F. D'Yvoire and M. Pintard-Screpel, *C. R. Acad. Sci., Ser. C*, 1980, **290**, 185.
3 C. C. Torardi and J. C. Calabrese, *Inorg. Chem.*, 1984, **23**, 1308.
4 P. Lightfoot, A. K. Cheetham, and A. W. Sleight, *J. Solid State Chem.*, 1988, **73**, 325.
5 P. Lightfoot and A. K. Cheetham, *J. Solid State Chem.*, 1989, **78**, 17.
6 P. Lightfoot and A. K. Cheetham, Abstracts, 3rd European Conf. Solid State Chemistry, Regensburg, 1986.
7 P. Lightfoot and A. K. Cheetham, *Acta Crystallogr., Sect. C*, 1988, **44**, 1331.
8 Yu. A. Gorbunov, B. A. Maksimov, Yu. K. Kabalov, A. N. Ivaschenko, O. K. Mel'nikov, and N. V. Belov, *Dokl. Akad. Nauk SSSR*, 1980, **254**, 873.
9 L. Koester and W. B. Yelon, Summary of Low Energy Neutron Scattering Lengths and Cross-Sections, Netherlands Energy Research Foundation, Department of Physics, Petten, 1982.
10 H. M. Rietveld, *J. Appl. Crystallogr.*, 1969, **2**, 65.
11 D. E. Cox, *Acta Crystallogr., Sect. A*, 1984, **40**, 369.
12 R. A. Young and D. B. Wiles, *J. Appl. Crystallogr.*, 1982, **15**, 430.
13 I. D. Brown and R. D. Shannon, *Acta Crystallogr., Sect. A*, 1973, **29**, 266.
14 A. R. Rae-Smith, A. J. Skarnulis, and P. W. Betteridge, Chemical Crystallography Laboratory, Oxford, 1980.
15 D. A. O. Hope and A. K. Cheetham, *J. Solid State Chem.*, 1988, **72**, 42.

Received 21*st September* 1988; *Paper* 8/03687J